



UNIVERSITY OF LEEDS

This is a repository copy of *Comparative in situ analysis reveals the dynamic nature of sclerenchyma cell walls of the fern Asplenium rutifolium*.

White Rose Research Online URL for this paper:
<http://eprints.whiterose.ac.uk/125739/>

Version: Accepted Version

Article:

Leroux, O, Eder, M, Saxe, F et al. (4 more authors) (2018) Comparative in situ analysis reveals the dynamic nature of sclerenchyma cell walls of the fern *Asplenium rutifolium*. *Annals of Botany*, 121 (2). pp. 345-358. ISSN 0305-7364

<https://doi.org/10.1093/aob/mcx167>

© 2017, The Author(s). Published by Oxford University Press on behalf of the Annals of Botany Company. This is a pre-copyedited, author-produced PDF of an article accepted for publication in *Annals of Botany* following peer review. The version of record: Olivier Leroux, Michaela Eder, Friederike Saxe, John W C Dunlop, Zoë A Popper, Ronald L L Viane, J Paul Knox; Comparative in situ analysis reveals the dynamic nature of sclerenchyma cell walls of the fern *Asplenium rutifolium*, *Annals of Botany*, Volume 121, Issue 2, 12 February 2018, Pages 345–358, is available online at: <https://doi.org/10.1093/aob/mcx167>

Reuse

Items deposited in White Rose Research Online are protected by copyright, with all rights reserved unless indicated otherwise. They may be downloaded and/or printed for private study, or other acts as permitted by national copyright laws. The publisher or other rights holders may allow further reproduction and re-use of the full text version. This is indicated by the licence information on the White Rose Research Online record for the item.

Takedown

If you consider content in White Rose Research Online to be in breach of UK law, please notify us by emailing eprints@whiterose.ac.uk including the URL of the record and the reason for the withdrawal request.



eprints@whiterose.ac.uk
<https://eprints.whiterose.ac.uk/>

ORIGINAL ARTICLE**Comparative *in situ* analysis reveals the dynamic nature of sclerenchyma cell walls of the fern *Asplenium rutifolium***

Olivier Leroux^{1*}, Michaela Eder², Friederike Saxe², John W.C. Dunlop², Zoë A. Popper³, Ronald L.L. Viane¹, J. Paul Knox⁴

¹Department of Biology, Ghent University, K.L. Ledeganckstraat 35, 9000 Gent, Belgium

²Department of Biomaterials, Max-Planck-Institute of Colloids and Interfaces, Wissenschaftspark Golm, Am Muhlenberg 1, 14476 Potsdam, Germany

³Botany and Plant Science and The Ryan Institute for Environmental, Marine and Energy Research, School of Natural Sciences, National University of Ireland Galway, Galway, Ireland

⁴Centre for Plant Sciences, Faculty of Biological Sciences, University of Leeds, Leeds LS2 9JT, UK

**For correspondence. E-mail Olivier.Leroux@UGent.be*

Running title: Collenchyma in ferns

ABSTRACT

- **Background and aims** A key structural adaptation of vascular plants was the evolution of specialised vascular and mechanical tissues, innovations likely to have generated novel cell wall architectures. While collenchyma is a strengthening tissue typically found in growing organs of angiosperms, a similar tissue occurs in the petiole of the fern *Asplenium rutifolium*.
- **Methods** The *in situ* cell wall (ultra)structure and composition of this tissue was investigated and characterized mechanically as well as structurally through nano-indentation and wide-angle X-ray diffraction, respectively.
- **Key results** Structurally the mechanical tissue resembles sclerenchyma, while its biomechanical properties and molecular composition both share more characteristics with angiosperm collenchyma. Cell wall thickening only occurs late during cell expansion or after cell expansion has ceased.
- **Conclusions** If the term collenchyma is reserved for walls that thicken during expansive growth, the mechanical tissue in *Asplenium rutifolium* represents sclerenchyma that mimics the properties of collenchyma and has the ability to modify its mechanical properties through sclerification. These results support the view that collenchyma does not occur in ferns and most likely evolved in angiosperms.

Key words: *Asplenium rutifolium*, collenchyma, mannan, nano-indentation, primary cell wall, secondary cell wall, sclerenchyma, septate fibres, xyloglucan

INTRODUCTION

The colonisation of land by plants marked a period of morphological diversification matched by equally impressive anatomical specialisation. By the middle Devonian, the development of complex vascular and mechanical tissues had facilitated plants to shift from reliance on the maintenance of turgor pressure to remain upright to a homoiohydric life style (Niklas & Speck, 2001; Ligrone *et al.*, 2012), which enabled plants to increase in height and develop complex growth forms. In extant land plants, mechanical support is provided by sclerenchyma and collenchyma (Evert, 2006). Collenchyma typically occurs in the peripheral regions of growing and/or herbaceous stems and petioles and consists of elongated cells with pectin-rich thickened primary cell walls, which are mainly deposited during elongation (Leroux, 2012). Sclerenchyma, contrastingly, is comprised of cells with lignified pectin-poor secondary cell walls, laid down after elongation has ceased (Evert, 2006). Although this classification is widely accepted, some tissues have been reported that do not comfortably fit within either of the above-mentioned definitions. For instance, collenchyma tissues may undergo lignification, making them undistinguishable from sclerenchyma. Some sclerenchyma tissues, on the other hand, may develop flexible, non-lignified pectin-rich cell walls which resemble collenchyma (see Leroux, 2012 for an overview). Moreover, non-lignified rigid cell walls have been reported in the fruit wall of *Nelumbo nucifera* (van Bergen *et al.*, 1997), showing that sclerenchyma cell walls do not necessarily contain lignin. To avoid confusion when referring to some types of mechanical tissue, alternative terms may be employed. The term ‘sclerified’ can be used to describe tissues that have developed rigid cell walls. As opposed to ‘lignified’ it does not imply the presence of lignin. The term ‘collenchymatous tissue’, originally coined by Esau (1936), can be employed to refer to tissues that structurally or

functionally resemble collenchyma. By using this term it is neither implied that the cells are elongated nor that they consist of primary and/or secondary cell walls (Leroux, 2012).

Whereas sclerenchyma can be found in most vascular plants, ‘true’ collenchyma tissues (i.e. with thickened pectin-rich primary cell walls deposited during elongation; henceforth referred to as ‘collenchyma’) are only known to occur in flowering plants, therefore appearing to be a more recent evolutionary innovation. However, collenchyma-like tissues have been reported in ferns and lycophytes (see Leroux, 2012 for an overview). Unfortunately, most of these studies do not provide compelling evidence and lack detailed information on either cell wall architecture or biomechanical properties.

During a comparative study of mechanical tissues in ferns collenchymatous tissues were observed in the petioles of *Asplenium rutifolium* (Aspleniaceae, leptosporangiate ferns) and related species such as *A. theciferum*, *A. loxoscaphoides*, *A. rutifolium* and *A. sandersonii*. These collenchymatous tissues provide flexibility to the petioles, allowing bending without breakage. In some of the larger leaves, however, parts of the collenchymatous tissue undergo sclerification, resulting in rigid petioles that break when bent. Species with small leaves (e.g. *A. sandersonii*) do not contain sclerified collenchymatous tissues.

In this paper we investigate the (ultra)structure, *in situ* cell wall composition and biomechanical properties of the collenchymatous tissue in the petiole of *Asplenium rutifolium* to determine to what extent this tissue conforms to the general characteristics typical of collenchyma found in angiosperms. We specifically chose to study *A. rutifolium* as some of its larger petioles contain both collenchymatous and sclerified

collenchymatous tissues, allowing comparison of the biomechanical properties of both types of mechanical tissue.

MATERIAL & METHODS

Plant material

Asplenium rutifolium was collected in South Africa (accession number RV11506) and kept in the living collection at the Ghent Botanic Garden, Belgium (<https://www.ugent.be/we/en/services/garden>).

Vibratome sectioning

Petiole segments were fixed overnight at 4°C in 4% v/v paraformaldehyde in PEM buffer (50 mM piperazine-N,N'-bis(2-ethanesulfonic acid), 5 mM MgSO₄ and 5 mM ethylene glycol tetraacetic acid, pH 6.9). Following fixation, the samples were washed in phosphate-buffered saline (PBS: prepared from a 10× stock solution — 80 g NaCl, 28.6 g Na₂HPO₄·12H₂O and 2 g KH₂PO₄ in 1 L de-ionised H₂O, pH 7.2) and subsequently mounted onto the vibratome stage using superglue (Loctite 406, Henkel Benelux). Transverse sections, 50 μm thick, were cut under water with a Microm HM650V vibration microtome (Microm International GmbH, Walldorf, Germany). Sections were either immunolabelled or stained with either Delafield's heamatoxylin (Johansen, 1940) or phloroglucinol-HCl and the Mäule reagent (Soukup, 2014) for anatomical analysis and for lignin detection, respectively.

Resin-embedding and sectioning for light microscopy

Plant material was fixed overnight in FAA (50% v/v ethanol, 5% v/v acetic acid and 5% v/v commercial formalin in distilled water), dehydrated in an ethanol series,

embedded in Technovit 7100 (Heraeus Kulzer, Wehrheim, Germany), sectioned, stained with toluidine blue and mounted as described by Leroux *et al.* (2007). Sections were observed with a Nikon Eclipse E600 microscope and images were recorded using a Nikon digital camera DXM1200.

Transmission electron microscopy

Plant material was fixed in 4% v/v paraformaldehyde and 2.5% v/v glutaraldehyde in 100 mM cacodylate-HCl buffer pH 6.9 for 24 h at 4°C, post fixed in 2% v/v osmium tetroxide for 2 h and dehydrated in an ethanol series at room temperature. For embedding in Spurr's low viscosity medium (Spurr, 1969), the samples were transferred to 100% Spurr's resin: absolute ethanol (1: 1) at 4°C for 9 h, brought to 100% Spurr's resin: absolute ethanol (2:1) for 8 h and left in 100% resin overnight at 4°C. Polymerisation was performed in flat embedding moulds at 70°C for 16 h. Sections, 70 nm thick, were made with a diamond knife on a Reichert Ultracut S microtome (Leica, Vienna, Austria), collected on copper mesh grids and stained with a Leica EM stainer (Leica, Vienna, Austria) for 30 min in 2% w/v uranyl acetate at 40°C and 10 min in Reynolds' lead citrate (Reynolds, 1963) at 20°C. All grids were examined with a Hitachi H7000 transmission electron microscope equipped with ATM digital image acquisition.

Scanning electron microscopy

Longitudinal hand-cut petiole segments were fixed in FAA, dehydrated in a graded ethanol series followed by a graded acetone series, and dried in a critical point dryer (Balzers CPD-030) using CO₂ as a transition fluid. Dried samples were mounted on aluminium stubs with double-sided adhesive graphite tabs. Mounted specimens were

coated with gold (12–15 nm thick) using a sputter coater (Balzers SPD-050). Sections were photographed digitally using an EVO40 scanning electron microscope (Carl Zeiss, Germany).

Immunocytochemistry

A range of specific cell wall-directed probes available from PlantProbes (<http://www.plantprobes.net/>) and Biosupplies (<http://www.biosupplies.com.au>) was used to evaluate the presence of major cell wall polymers including cellulose (CBM3a; Blake *et al.*, 2006), pectic homogalacturonan (LM19, LM20; Verhertbruggen *et al.*, 2009), (1→5)- α -arabinan (LM6; Willats *et al.*, 1998), (1→4)- β -galactan (LM5; Jones *et al.*, 1997), xyloglucan (LM15; Marcus *et al.*, 2008; LM25; Pedersen *et al.*, 2012), heteroxylan (LM10, LM11; McCartney *et al.*, 2005), heteromannan (LM21, Marcus *et al.*, 2010), (1→3)(1→4)- β -D-glucan (BioSupplies 400-3; Meikle *et al.*, 1994) and callose (Biosupplies 400-2; Meikle *et al.*, 1991). Vibratome sections were incubated in 5% w/v non-fat milk protein in PBS (MP/PBS) for 5 min to block non-specific binding sites. Sections were then incubated with primary rat monoclonal antibodies (mAbs) (LM19, LM20, LM5, LM6, LM10, LM11, LM15, LM25, LM21) diluted 1:10 in MP/PBS for 1 h. The sections were washed with several changes of PBS prior to incubation with the secondary antibody, anti-rat-IgG linked to fluorescein isothiocyanate (FITC; Sigma) diluted 1:100 in 5% w/v MP/PBS for 1 h. The binding of CBM3a (Blake *et al.*, 2006) was assessed by a three-stage immunolabelling procedure (Hervé *et al.*, 2011). After incubating in MP/PBS containing 25 μ g/ml of CBM3a protein for 1.5 h, sections were washed in PBS at least three times and incubated with a

100-fold dilution of mouse anti-his monoclonal antibody (Sigma) in MP/PBS for 1.5 h. Following washing with PBS, anti-mouse-IgG linked to fluorescein isothiocyanate (FITC; Sigma) was applied for 1.5 h as a 50-fold dilution in MP/PBS. Immunolabelling with the BioSupplies 400-2 and 400-3 mouse mAbs was performed as described by Meikle *et al.* (1994). Both primary antibodies were diluted 1:50. Cellulose was stained with Calcofluor White M2R fluorochrome (Fluorescent brightener 28, Sigma, 0.25 $\mu\text{g mL}^{-1}$ in dH_2O) for 5 min. After incubation with a secondary antibody, anti-mouse-IgG linked to fluorescein isothiocyanate (FITC; Sigma), all sections were washed in PBS three times before mounting in a glycerol-based anti-fade solution (Citifluor AF2, Citifluor Ltd., UK). As some cell wall epitopes may be masked by pectic homogalacturonan we performed pectate lyase pretreatments as described by Marcus *et al.* (2008). Immunofluorescence was observed with a microscope equipped with epifluorescence irradiation (Olympus BX-61) and the following filter cubes: excitation 365/15BP; dichroic mirror 400LP; emission 420LP for visualizing Calcofluor White stained cell walls; excitation 480/20BP; dichroic mirror 505LP; emission 410LP for green emission of the FITC fluorochrome, and, excitation 535/30BP; dichroic mirror 565LP; emission 580LP 541/572nm for imaging red autofluorescence of brown-coloured sclerified cell walls (henceforth referred to as 'red autofluorescence'). Images were captured with a Hamamatsu ORCA285 camera and processed with Perkin Elmer Volocity software.

Microfibril angle measurements

Longitudinal fibre bundles ($\sim 0.2 \times 0.5 \times 3 \text{ mm}^3$) of collenchymatous and sclerified collenchymatous tissue (n=5 respectively) were mounted on a metal sample holder. Wide-angle X-ray diffraction experiments were performed with a Nanostar (Bruker

AXS) instrument using $\text{CuK}\alpha$ radiation with a wavelength of 1.54\AA . The sample-detector distance was 5.5 cm. For each measurement point diffraction patterns were collected in vacuum for 2×60 min with at 2D Vantec 2000 detector (Fig. 5D,E). The exact sample-detector distance and the beam centre were determined with the software Fit2D (Hammersley 1998) through the powder measurement of a corundum standard with known peak positions. The measurement files were corrected for background scattering by subtraction of an empty beam measurement of 60 min. The files were integrated azimuthally from 0° – 360° (radial profile, Fig. 5F) to determine the position of the 200 Bragg peak of cellulose on the detector. The same data was then radially integrated in the range of the 200 cellulose peak ($Q = 14.3$ – 16.3°) to obtain an azimuthal scattering profile (Fig. 5G). For integration the software Autofit, a Python based software developed by Chenghao Li, Aurelien Gourrier and Gerald A. Zickler at the Max-Planck-Institute of Colloids and Interfaces in Potsdam was used. The duplicate measurements of each measurement point were averaged. Besides the crystalline cellulose, amorphous non-oriented components contribute to the scattering signal. To correct for this type of background scattering, the slope of a line connecting two points outside the cellulose Bragg peaks ($Q = 8.5$ and $Q = 18.9$) was determined and set as baseline. Then, the baseline intensity could be determined for the range of the 200 Bragg peak and was subtracted from the azimuthal scattering profile. In a microfibril angle simulation (Rüggeberg *et al.*, 2013), the microfibril angle distribution is approximated by two Gauss peaks (Fig. 5H) such that the according scattering profile is fitted to the measured azimuthal scattering profile.

Nanoindentation experiments

Approximately 3–5 mm long segments, cut exactly 90 degrees to the longitudinal petiole axis were sequentially dehydrated by a graded ethanol series. The segments were put in methyl methacrylate (MMA, Sigma aldrich) for 48 h. After 24 h the solution was exchanged with fresh solution. On the third day the samples were put in infiltration solution (150 ml MMA, 10 ml nonylphenyl-polyethyleneglycol acetate (NPO, Sigma aldrich) and 1 g benzoylperoxide blend (BPO) with dicyclohexylphthalate (Sigma Aldrich)) for at least 24 h. Prior to the final embedding step the samples were glued with the cross section on a metal AFM specimen holder to ensure alignment. The metal plate fixed sample was placed in a mould and covered with PMMA (polymethylmethacrylate) solution made of 100 ml MMA, 25 ml NPO and 2.0 g BPO. For PMMA polymerization the samples were placed in an oven for 24 h at 40°C, followed by 24 h at 48°C and then 24 h at 55°C. After polymerization samples were polished parallel to the metal holder to create collenchyma and sclerified collenchymatous cell wall cross sections exactly 90 degrees to the longitudinal petiole axis.

On the polished samples, walls of 11 collenchymatous and 12 sclerified collenchymatous cells were probed with a Berkovich indenter. Collenchymatous cell walls were indented with a peak load of 150 μN . Load application for 2.5 sec was followed by a 15 sec holding segment and then by a 2.5 sec unloading segment (Fig. 6A). The same load function, but with a peak load of 350 μN (Fig. 6B), was used to indent sclerified collenchymatous cell walls, to have comparable indentation depths of ~200 nm for the two cell types. After indentation the positions of all indents were controlled to ensure that they were placed in the cell walls. Indentation moduli (or

reduced moduli E_r) were calculated according to the relationship

$$E_r = \frac{1}{\beta \sqrt{A_{\max}}} \left. \frac{dP}{dh} \right|_{h_{\max}}$$

(Oliver and Pharr, 1992). β is an indenter shape dependent factor, A_{\max} the projected contact area under load between indenter and cell wall and dP/dh is the initial unloading slope (Fig. 6C), Hardness was determined as the ratio between the maximum load P_{\max} and the residual indent area A_r .

Mechanical modeling

Twelve vibratome cross sections of the petiole and rachis of a large *Asplenium rutifolium* (accession number RV11506) leaf were made at 3 cm intervals from the base and imaged. These images were then segmented by hand into regions of parenchyma, collenchymatous and collenchymatous sclerified tissue (Fig. 7A). Segmented images were imported into Matlab *R2015b* and the local bending rigidity was determined using a custom made code implementing standard equations (Gere, 2002). One fern petiole was cut into twelve 3-cm long segments (Fig. 1) and each segment weighed, giving data about the self-loading of each segment (data not shown). This data was then used to calculate deflections and rotations of each segment as a function of self-load using simple beam theory, assuming small deflections. The deflections and rotations of each segment were combined using the principle of superposition to calculate tip deflection under self-load for horizontally oriented petioles both with and without sclerification (Gere, 2002).

RESULTS

Distribution, structure and development of mechanical tissue in *A. rutifolium* petioles

Figure 1 displays cross sections through different regions along the petiole and rachis of a large *Asplenium rutifolium* leaf. All sections contain subepidermal collenchymatous tissue of which some parts are sclerified, depending on the position in the leaf. At the petiole base strands of sclerified collenchymatous tissue intersperse the collenchymatous tissue at the adaxial and abaxial side. In the upper half of the leaf, sclerified collenchymatous tissue is absent. A higher magnification of a section through the petiole base is shown in Figure 1B. While collenchymatous tissue is comprised of uniformly thickened cell walls that are translucent in unstained sections, sclerified collenchymatous tissues have yellow to brown coloured cell walls. During sclerification the collenchymatous cell walls are impregnated with yellow to brown pigments and additional cell wall material is deposited, resulting in unevenly thickened cell walls (Fig. 1B). Sclerification is initiated at the abaxial side of the petiole base and extends towards the rachis. Initially, strands of dark brown sclerified tissues are formed (Fig. 1B) and in some cases all of the collenchymatous tissue at the petiole base becomes sclerified while collenchymatous tissues remain higher up in the leaf. The petiole base of small leaves does not contain sclerified collenchymatous tissue (Fig. 2a). The peripheral collenchymatous tissue is only interrupted by parenchyma where respiration lines with stomata run along both sides of the petiole (Fig. 2a). Longitudinal sections show that collenchymatous cells are narrow and elongated with tapered ends (Fig. 2B). These cells are in turn subdivided by one to four thin-walled septae, with a nucleus in each compartment (Fig. 2C). To determine whether the mechanical tissue consists of primary and/or secondary cell walls we compared transverse sections through different segments of a fern crozier. Uncoiling of fern croziers is accomplished by differential growth, with the cells located abaxially elongating to a lesser extent. Cells in crozier segments just below the coil have ceased or almost finished their expansion growth. A

transverse section through the latter segment shows that the walls of the collenchymatous cells are not yet fully differentiated and resemble the primary walls of the ground parenchyma cells in terms of cell wall thickness (Fig. 2D). In transverse sections of mature collenchymatous tissue, on the other hand, two distinct wall layers are observable: a thin outer layer which corresponds to the primary cell walls as seen in undifferentiated tissue, and a thick, weakly stained layer which constitutes the secondary cell wall (Fig. 2E), as it is most likely deposited after elongation has ceased. It is of interest to note that, if we distinguish primary and secondary walls as such, a thin secondary wall is also deposited in the cells of the parenchymatous ground tissue (Fig. 2E).

In situ cell wall composition of mature collenchymatous cells indicates primary cell wall architecture

To examine the presence and location of major cell wall components, we immunolabelled vibratome sections through small petioles containing mature collenchyma (sections equivalent to Fig. 2A) with a range of mAbs and a carbohydrate-binding module (CBM). Sections were also stained with Calcofluor White, a dye with a high affinity for β -D-glucans (Fig. 3A); employed here to show the full extent of cell walls. CBM3a, recognizing crystalline cellulose, bound to all tissues, including the collenchymatous cell walls (Fig. 3B). We used two mAbs which recognize pectic homogalacturonan (HG) either with low (LM19) or high (LM20) levels of methyl-esterification. The LM19-epitope was detected in the collenchymatous and

parenchymatous cell walls (Fig. 3C, E). LM20, on the other hand, strongly labelled the lining of intercellular spaces of the cortical parenchyma, but only weakly bound to the collenchymatous tissue (Fig. 3D, F). LM5, directed against (1→5)-β-galactan, labelled the inner cell wall layer of collenchymatous cells (Fig. 3G) including the septae (Fig. 3G, inset). The LM6 mAb, recognizing (1→5)-α-L-arabinan, did not bind to the collenchymatous cell walls (Fig. 3H), but was detected in the vascular bundles and epidermal cell walls, and, after pectate lyase treatment, also labelled the intercellular space linings of the cortical parenchyma (data not shown). The anti-xylan mAbs LM10 and LM11 did not bind to the collenchymatous cell walls (data not shown). The anti-mixed-linkage glucan antibody (BioSupplies 400-3) bound to the inner cell wall layer of the collenchymatous cells (Fig. 3I). LM25, a mAb recognizing the XXXG and galactosylated structural motifs of xyloglucan, bound to parenchymatous and collenchymatous walls and the fluorescence signal was stronger in the inner wall layers (Fig. 3J). The LM15 anti-xyloglucan mAb, which binds to the XXXG and XXGG motif, displayed a rather unusual binding pattern in collenchymatous cells after pectate lyase treatment as the epitope is restricted to the three-way junctions of the collenchymatous tissue (Fig. 3K–M). Binding of the LM15 mAb was rather weak and therefore increased exposure times were used to image the labelling pattern. Pectate lyase unmasked the LM21 heteromannan epitope in the primary cell walls of the collenchymatous and parenchymatous cell walls of the cortex (Fig. 4A–D). LM21 did not bind to the septae of the collenchymatous walls (Fig. 4E, F).

Of all mAbs used, only LM21 bound to sclerified collenchymatous cell walls, with labelling being restricted to a thin inner cell wall layer (Fig. 4H). Sclerification was seen to coincide with phenolic impregnation which hinders Calcofluor White staining (Fig. 4G) and causes autofluorescence in the red channel (Fig. 4I). In some

collenchymatous cell walls we observed binding of LM21 to the inner cell wall layers (Fig. 4K). The absence of autofluorescence (Fig. 4L) suggests that these walls are not impregnated with phenolic compounds. This may imply that, during sclerification, deposition of mannan precedes phenolic impregnation.

Collenchymatous tissues were not stained with the Wiesner and Mäule reagents (data not shown). These dyes only reacted with xylem tracheid walls, indicating the presence of lignin. Interpretation of lignin staining in sclerified collenchymatous tissues, however, was obscured due to the dark brown pigmentation of the cell walls.

Ultrastructural imaging reveals the polylamellated nature of collenchymatous cell walls

Transmission electron microscopy showed that the walls of the collenchymatous tissue are polylamellated (Fig. 5A). Higher magnifications indicated that the fibril orientation changes in successive lamellae and that low and high electron-dense lamellae alternate (Fig. 5B). The walls of the septae are thin and their middle lamellae are not fused with those of the collenchymatous mother cells. A three-way junction between the newly formed compartments and the mother cell is therefore not formed. The walls of the septae also appear to be continuous with an inner wall layer of the collenchymatous mother cells (Fig. 5B). A transverse section through sclerified collenchymatous tissue (Fig. 5C) shows the original collenchymatous secondary walls (designated as layer '1') as well as newly deposited secondary cell wall layers (designated as layers '2' and '3'). The increased electron density of cell wall layers '1' and '2' results from impregnation with yellow- brown pigments. As layer '3' appears to be more electron lucent, it is most likely not impregnated with the latter pigments.

The anti-callose mAb specifically bound to the transverse walls and septae of the cortex parenchyma and the collenchymatous tissue respectively (Fig. S1A). Scanning and transmission electron microscopy (TEM) of these transverse cell walls showed that they were densely pitted (Fig. S1B–E). The dotted labelling pattern suggests that callose is deposited in association with these pits.

Comparable cellulose microfibril angles in collenchymatous and sclerified cell walls

Wide-angle X-ray scattering experiments support the TEM finding that cellulose orientation changes in successive cell wall layers. Both non-sclerified and sclerified collenchymatous cell walls show two main cellulose orientations. In non-sclerified collenchymatous cell walls cellulose fibrils are oriented at 8° (~57%) and 62° (~43%) (Fig. 5H) to the longitudinal cell axis. The microfibril angle in cell walls of sclerified tissue was calculated to be 9° (52%) and 60° (48%) (Fig. 5G). Even though a scattering signal of higher intensity (Fig. 5F) was observed for the sclerified tissue, no significant differences in the azimuthal scattering profile and the resulting cellulose orientation distributions were found between non-sclerified and sclerified cells (Fig 5 G,H).

Nanoindentation experiments indicate differences in mechanical properties

The average indentation modulus (Fig. 6D) in collenchymatous cell walls was 7.29 GPa (n=34) and in sclerified cells 13.51 GPa (n=97). More indents were placed in sclerified cells to study if mechanical properties change from the middle lamellae to the lumina. However, no clear differences could be found. Compared to the almost 2-fold higher stiffness in sclerified cells, hardness values increased even more: collenchymatous cells reached mean hardness values of 142.8 MPa and sclerified collenchymatous cells 391.7 MPa (Fig. 6E).

DISCUSSION

Collenchymatous tissue of A. rutifolium structurally resembles sclerenchyma tissue

Collenchyma tissues can generally be recognized by their uneven deposition of cell wall material either in cell corners (angular collenchyma) or on the inner and outer tangential cell walls (plate collenchyma) (Leroux, 2012). However, in some cases plants contain collenchyma characterized by more uniformly thickened cell walls (annular collenchyma) and, as such, distinction from sclerenchyma tissue is not straightforward if only structural characteristics are considered. This is the case for the mechanical tissue in the petiole of the fern *Asplenium rutifolium*, a pliable tissue with uniformly thickened cell walls that may undergo sclerification. Additional microscopic observations of the latter tissue indicated other diagnostic structural features including elongated cell shape, tapered cell ends and the presence of septae. Yet, these features can also not be employed to distinguish between collenchyma and sclerenchyma as they may apply to both types of mechanical tissue (Leroux, 2012).

One of the characteristics that clearly sets collenchyma apart from sclerenchyma is that collenchyma initiates cell wall thickening during the early phases of expansion, while sclerenchyma only deposits cell walls after expansion has ceased (Leroux, 2012). In *A. rutifolium*, collenchymatous walls were shown to be deposited after or during the last phases of elongation. For this reason, the latter walls are secondary cell walls and, hence, the mechanical tissue should be referred to as sclerenchyma. This might explain why a distinctive primary wall was observed, as only this wall needs to cope with extensive elongation and may have a different chemical composition altering its affinity for dyes such as toluidine blue. In collenchyma, a thin, easily distinguished outer cell wall layer is generally not observed.

Collenchymatous tissue of A. rutifolium has a similar cell wall composition to angiosperm collenchyma

Comparison of tissue-specific cell wall composition between representatives of different plant groups is not straight-forward. The abundance and relative proportions as well as the fine-structural details of cell wall polysaccharides may vary between the major groups of land plants (Fangel *et al.*, 2012). Moreover, differences in composition do not necessarily imply differences in properties as different configurations of plant wall polymers may generate walls with similar properties. While analysis of fractionated walls of isolated collenchyma tissues (as performed on celery collenchyma by Chen *et al.*, 2017) of several plants will allow a better overview of the variation in collenchyma cell wall composition, the immunocytochemical experiments performed in this study allowed investigation and comparison of the spatial distribution of glycan epitopes. Our results show that the collenchymatous cell walls of *A. rutifolium* are rich in cellulose, xyloglucan and pectic HG, both of which are characteristic of angiosperm collenchyma walls (Jarvis, 2007; Chen *et al.*, 2017). The prevalence of the LM19 epitope over the LM20 epitope in the collenchymatous cell walls suggests the presence of continuous stretches of de-esterified (rather than esterified) HG, which may be involved in the formation of strengthening calcium-mediated pectic gels (Albersheim *et al.*, 2010). The LM5 mAb, directed against (1→4)- β -D-galactan, which occurs as side-chains of pectic rhamnogalacturonan-I in angiosperms, only labelled the inner cell wall layers and the septae of the collenchymatous cells in *A. rutifolium*. These galactan-rich layers most likely correspond to the distinct inner layer that is continuous with the septae walls as seen by TEM. Similar distribution patterns of the LM5 galactan epitope, being restricted to the inner cell wall layers, were observed in collenchyma of tomato

petioles (Jones *et al.*, 1997), hemp stems (Blake *et al.*, 2008) and elderberry stems (Leroux, 2012), suggesting that galactan might play an important role in the differentiation process of collenchymatous tissues. Several reports have suggested that pectic galactan is correlated with cells that undergo extensive elongation. For example, galactans were shown to be present in primary cell walls of elongating cells of potato stolons (Bush *et al.*, 2001) and in elongating carrot suspension cells (Willats *et al.*, 1999). In ferns, galactans have been immunodetected in the cell walls of sieve tube cells, which also undergo extensive elongation (Leroux *et al.*, 2015).

Cell walls of representatives of different plant groups were shown to contain different proportions of hemicelluloses (Harris, 2005). Compared to angiosperms, fern primary cell walls were reported to be particularly rich in mannans (Popper and Fry, 2004; Silva *et al.*, 2011). In *Asplenium rutifolium*, mannan-epitopes were detected after pectate lyase treatment in all primary cell walls of the cortex, including those of the mechanical tissue. We immunodetected xyloglucan in the collenchymatous thickenings using the LM25 mAb to XXXG/galactosylated epitopes. Xyloglucans have been identified as one of the main hemicellulosic polysaccharides in eudicot angiosperm primary cell walls (Cosgrove, 2005), and xyloglucan epitopes have been localised in angiosperm collenchyma cell walls (Marcus *et al.*, 2008). While the xylan-directed mAbs LM10 and LM11 bound to discrete zones in tobacco collenchyma after enzymatic removal of HG (Hervé *et al.*, 2009), they did not bind to collenchymatous cell walls in *A. rutifolium* and removal of pectic HG did not affect their binding pattern. Mixed-linkage glucan epitopes were detected in the innermost layer of collenchymatous tissues. This polysaccharide was previously reported to occur in leptosporangiate ferns by Leroux *et al.* (2015) where it was also detected in collenchymatous thickenings of *Equisetum arvense*. Further analyses, however, are

necessary to biochemically determine the structure of the cell wall component that binds to the BS-400-3 mAb in *A. rutifolium*. While our results indicate that collenchymatous tissue in *A. rutifolium* shows similarities with angiosperm collenchyma, more collenchymatous tissues across vascular plants should be investigated to reveal the range of variation in cell wall composition.

Septae are formed after secondary cell wall deposition

As the septae form junctions with the secondary cell walls of the parent cells, they must arise from divisions of the protoplast of mature collenchymatous cells that have already developed wall thickenings and not of initial cells of the apical shoot meristem. The galactan-rich inner cell wall layer of the collenchymatous parent cell, which was found to be continuous with the primary cell walls of the septae, is most likely deposited by the protoplast during cytokinesis. Considering that the septae only appear late during mechanical tissue differentiation it is not surprising that these transverse cell walls display a distinct cell wall composition. For instance, LM21 mannan epitopes were only detected in the primary walls of the cell files that originated from the collenchymatous initial cells and were not found in the septae.

Mannans are implicated in the sclerification process of collenchymatous tissues

Mannans have been identified as the major components of secondary cell walls in gymnosperms and ferns (Whistler and Chen, 1991; Bremner and Wilkie, 1971; Timell, 1962) and have been immunodetected in fern sclerenchyma tissues (Leroux et al., 2015). In *A. rutifolium*, the anti-mannan probe LM21 bound to the inner cell wall layer, most likely corresponding to the electron-lucent inner layer revealed by transmission electron microscopy, of sclerified collenchymatous cells. None of the mAbs used in this

study bound to the secondary cell wall layers that were shown to be electron dense by TEM (i.e. layers '1' and '2', Fig. 5C). A possible explanation is that glycan epitopes are masked as a result of pigment impregnation. Our results also revealed that incorporation of mannan appears to precede phenolic impregnation (Fig. 4), suggesting that mannans may play a crucial role in the sclerification process. We obtained no evidence for the presence of lignin in the mechanical tissue of *A. rutifolium*. This is not uncommon in ferns as biomechanical studies of extant *Equisetum* species, which also contain sclerifying collenchymatous tissues, have shown that lignification is not a prerequisite for conferring stiffness to plant tissues (Rowe and Speck, 2004). For instance, non-lignified rigid cell walls may be formed through a polysaccharide-tannin complex such as that found in the fruit wall of *Nelumbo nucifera* (van Bergen *et al.*, 1997). The polysaccharide fraction of these walls was predominantly composed of galactose and mannose residues and in combination with insoluble tannins, this wall complex might provide specific mechanical properties in a similar way as ligno-cellulosic composites.

The results of the nanoindentation experiments show that sclerification changes the mechanical properties of the cell walls considerably. Since the cellulose orientation in both collenchymatous and sclerified collenchymatous tissue is the same (Fig. 5F–H) effects coming from varying cellulose fibril orientations can be excluded (Konnerth *et al.*, 2009, Jäger *et al.*, 2011). The observed changes in mechanical properties can therefore be assigned to the incorporation of new or modification of existing cell wall components during the sclerification process. However, the indentation modulus of sclerified cell walls is in the lower range of what is found for lignified wood cell walls with small microfibril angles (Eder *et al.*, 2013). Possibly this can be explained by the multi-layered cell wall structure with a considerable percentage of fibrils being aligned

at rather high microfibril angles. Lignified multi-layered bamboo cell walls (Parameswaran and Liese, 1976) typically also show lower indentation moduli (e.g. Dixon and Gibson, 2014) than the S2 layer of wood cell walls.

The role of sclerification on the bending rigidity of petioles was estimated assuming sclerified tissue had four times the elastic modulus of the unsclerified tissue. This estimate is based on the two times higher indentation modulus and the approximately 2-fold higher cell wall proportion in an average cross section of sclerified tissue compared to collenchymatic tissue (Fig. 2F). Although occurring only in a small fraction of the tissue cross section sclerification rigidifies petioles significantly (Fig. 7B), especially close to the base, where the greatest bending moments are experienced (Fig. 1). This mechanical role of sclerification was further supported by calculations using standard beam theory (Gere, 2002), which showed that sclerification decreased the deflection of the tip of the petiole under self-loading by 21%.

Conclusions

The collenchymatous tissue in *A. rutifolium* petioles structurally resembles sclerenchyma, while in biomechanical performance and glycan composition it shares more characteristics with angiosperm collenchyma. If we reserve the term collenchyma for walls that (for the most part) thicken during expansive growth of organs, then the mechanical tissue in *Asplenium rutifolium* and related species represents sclerenchyma. This sclerenchyma tissue is highly versatile as its secondary cell walls mimic the properties of collenchyma walls and have the ability to modify their mechanical properties through sclerification. Such compositional and biomechanical dynamics might be essential as ferns cannot produce secondary tissues and therefore only rely on

the modification of their primary tissues to adjust the biomechanical performance of their organs.

Our results are in line with the present conjecture that collenchyma does not occur in ferns and most likely evolved in angiosperms. Although confusion remains regarding the precise definition of collenchyma, our results strengthen the view that cell walls are dynamic and can impart specific properties no matter when they are deposited. However, there are some architectural restrictions which apply as long as cell walls need to retain the ability to expand as sclerification will hinder this process. The challenge is not to define tissues but to understand how the observed molecular diversity underpins wall properties and functions.

SUPPLEMENTARY DATA

Supplementary data are available online at www.aob.oxfordjournals.org and consist of **Figure S1**. Immunodetection of callose and ultrastructure of the septae of collenchymatous tissue in *A. rutifolium*.

ACKNOWLEDGEMENTS

The Electron Microscopy Facility (Centre for Microscopy and Imaging, Anatomy School of Medicine, NUI Galway) and Pierce Lalor are acknowledged for providing assistance with sample preparation and imaging. We thank Ingrid Zenke for support during the X-ray measurements. We thank Agnieszka Bagniewska-Zadworna for assistance with scanning electron microscopy. This study was supported by the Fund for Scientific Research —Flanders, Belgium (F.W.O. — Vlaanderen) through a postdoctoral fellowship (12H8816N) and research grant (1524914N) provided to OL.

REFERENCES

- Albersheim P, Darvill A, Roberts K, Sederoff R, Staehelin A. 2010.** Plant Cell Walls: From Chemistry to Biology. Garland Science, New York.
- Blake AW, McCartney L, Flint JE, Bolam DN, Boraston AB, Gilbert HJ, Knox JP. 2006.** Understanding the biological rationale for the diversity of cellulose-directed carbohydrate-binding modules in prokaryotic enzymes. *Journal of Biological Chemistry* **281**: 29321–29329.
- Blake AW, Marcus SE, Copeland JE, Blackburn RS, Knox JP. 2008.** *In-situ* analysis of cell wall polymers associated with phloem fibre cells in stems of hemp, *Cannabis sativa* L. *Planta* **228**: 1–13.
- Bremner I, Wilkie KCB. 1971.** The hemicelluloses of bracken. II. A galactoglucomannan. *Carbohydrate Research* **20**: 193–203.
- Bush MS, Marry M, Huxham IM, Jarvis MJ and McCann MC. 2001.** Developmental regulation of pectic epitopes during potato tuberisation. *Planta* **213**: 869–880.
- Chen D, Harris PJ, Sims IM, Zujovic Z, Melton LD. 2017.** Polysaccharide compositions of collenchyma cell walls from celery (*Apium graveolens* L.) petioles. *BMC Plant Biology* **17**: 104.
- Cosgrove DJ. 2005.** Growth of the plant cell wall. *Nature Reviews Molecular Cell Biology* **6**: 850–861.
- Dixon PG, Gibson LJ. 2014.** The structure and mechanics of Moso bamboo material. *Journal of the Royal Society Interface* **11**: 20140321.
- Eder M, Arnould O, Dunlop JWC, Hornatowska J, Salmén L. 2013.** Experimental micromechanical characterization of wood cell walls. *Wood Science and Technology* **47**: 163-182.

Esau K. 1936. Ontogeny and structure of collenchyma and of vascular tissues in *celery* petioles. *Hilgardia* **10**: 431–476.

Evert RF. 2006. *Esau's plant anatomy. Meristems, cells, and tissues of the plant body: their structure, function, and development.* 3rd edition. New Jersey: John Wiley and Sons, Inc.

Fangel JU, Ulvskov P, Knox JP, Mikkelsen MD, Harholt J, Popper ZA, Willats WG. 2012. Cell wall evolution and diversity. *Frontiers in Plant Science*. doi: 10.3389/fpls.2012.00152.

Gere JM. 2002. *Mechanics of Materials*, 5th Edition, Nelson Thornes Press, Cheltenham.

Hammersley A. 1998. FIT2D V9.129 Reference Manual V3.1. ESRF Internal Report, ESRF98HA01T.

Harris PJ. 2005. Diversity in plant cell walls. In: Henry RJ, ed. *Plant diversity and evolution: genotypic and phenotypic variation in higher plants.* Wallingford: CAB International Publishing, 201–227.

Hervé C, Marcus SE, Knox JP. 2011. Monoclonal antibodies, carbohydrate-binding modules, and the detection of polysaccharides in plant cell walls. Chapter 7 p. 103–113. In: Popper ZA (ed.) *The Plant Cell Wall: Methods and Protocols.* Methods in Molecular Biology vol. 715. Springer, New York.

Jaeger A, Bader T, Hofstetter K, Eberhardsteiner J. 2011. The relation between indentation modulus, microfibril angle, and elastic properties of wood cell walls. *Composites Part A: Applied Science and Manufacturing* **42**: 677–685.

Jarvis MC. 2007. *Collenchyma.* In: Roberts K, ed. *Handbook of Plant Science*, John Wiley & Sons, Chichester, UK, p. 187–190.

- Johansen DA. 1940.** *Plant Microtechnique*. MacGraw-Hill Comp. Book Inc., London,
- Jones L, Seymour GB, Knox JP. 1997.** Localization of pectic galactan in tomato cell walls using a monoclonal antibody specific to (1→4)-β-D-galactan. *Plant Physiology* **113**: 1405–1412.
- Leroux O, Knox JP, Leroux F, Vrijdaghs A, Bellefroid E, Borgonie G, Viane RLL. 2007.** Intercellular Pectic Protuberances in *Asplenium*: new data on their composition and origin. *Annals of Botany* **100**: 1165–1173.
- Leroux O, Van der Kinderen G, Viane RLL. 2007.** A sandwich-embedding method for oriented sectioning. *Journal of Microscopy* **227**: 79–82.
- Leroux O, Sørensen I, Marcus SE, Viane RLL, Willats WGT, Knox P. 2015.** Antibody-based screening of cell wall matrix glucans in ferns reveal taxon, tissue, and cell-type specific distribution patterns. *BMC Plant Biology* **15**: 56.
- Leroux O. 2012.** Collenchyma: a versatile mechanical tissue with dynamic cell walls. *Annals of Botany* **110**: 1083–1098.
- Ligrone R, Duckett JG, Renzaglia KS. 2012.** Major transitions in the evolution of early land plants: a bryological perspective. *Annals of Botany* **109**: 851–871.
- Marcus SE, Blake AW, Benians TAS, Lee KJD, Poyser C, Donaldson L, Leroux O, Rogowski A, Petersen HL, Boraston A, Gilbert HJ, Willats WGT, Knox JP. 2010.** Restricted access of proteins to mannan polysaccharides in intact plant cell walls. *Plant Journal* **64**: 191–203.
- Marcus SE, Verhertbruggen Y, Hervé C, Ordaz-Ortiz JJ, Farkas V, Pedersen HL, Willats WGT, Knox JP. 2008.** Pectic homogalacturonan masks abundant sets of xyloglucan epitopes in plant cell walls. *BMC Plant Biology* **8**: 60. doi:10.1186/1471-2229-8-60

McCartney L, Marcus SE, Knox JP. 2005. Monoclonal antibodies to plant cell wall xylans and arabinoxylans. *Journal of Histochemistry and Cytochemistry* **53**: 543–546.

Meikle PJ, Bonig I, Hoogenraad NJ, Clarke AE, Stone BA. 1991. The location of (1→3)- β -glucans in the cell walls of pollen tubes of *Nicotiana alata* using a (1→3)- β -glucan-specific monoclonal antibody. *Planta* **185**: 1–8.

Meikle PJ, Hoogenraad NJ, Bonig I, Clarke AE, Stone BA. 1994. A (1→3,1→4)-beta-glucan-specific monoclonal antibody and its use in the quantitation and immunocytochemical location of (1→3,1→4)-beta-glucans. *The Plant Journal* **51**: 1–9.

Niklas KJ, Speck T. 2001. Evolutionary trends in safety factors against wind-induced stem failure. *American Journal of Botany* **88**: 1266–1278.

Oliver WC, Pharr GM. 1992. An improved technique for determining hardness and elastic modulus using load and displacement sensing indentation experiments. *J. Mater. Res.* **7**: 1564–1583.

Parameswaran N, Liese W. 1976. On the fine structure of bamboo fibres. *Wood Science and Technology* **10**: 231–246.

Pedersen HL, Fangel JU, McCleary B, Ruzanski C, Rydahl MG, Ralet M-C, Farkas V, von Schantz L, Marcus SE, Andersen MCF, Field R, Ohlin M, Knox JP, Clausen MH, Willats WGT. 2012. Versatile high-resolution oligosaccharide microarrays for plant glycobiology and cell wall research. *Journal of Biological Chemistry* **287**: 39429–39438.

Popper ZA, Fry SC. 2004. Primary cell wall composition of pteridophytes and spermatophytes. *New Phytologist* **164**: 165–174.

Reynolds ES. 1963. The use of lead citrate at high pH as an electron-opaque stain in electron microscopy. *Journal of Cell Biology* **17**: 208–212.

- Rowe N, Speck T. 2004.** Hydraulics and mechanics of plants: novelty, innovation and evolution. In: Hemsley AR, Poole I, eds. *The Evolution of Plant Physiology*. Academic Press, London.
- Rueggeberg M, Saxe F, Methger TH, Sundberg B, Fratzl P, Burgert I. 2013.** Enhanced cellulose orientation analysis in complex model plant tissues. *Journal of Structural Biology* 183: 419–428.
- Silva GB, Ionashiro M, Carrara TB, Crivellari AC, Tiné MA, Prado J, Carpita NC, Buckeridge MS. 2011.** Cell wall polysaccharides from fern leaves: Evidence for a mannan-rich Type III cell wall in *Adiantum raddianum*. *Phytochemistry* 72: 2352–2360.
- Soukup A. 2014.** Selected simple methods of plant cell wall histochemistry and staining for light microscopy. In: Žárský V, Cvrčková F. *Plant cell morphogenesis: Methods and Protocols*. Methods in Molecular Biology vol. 1080. Springer, New York.
- Spurr AR. 1969.** A low-viscosity epoxy resin embedding medium for electron microscopy. *Journal of Ultrastructural Research* 26: 31–43.
- Timell TE. 1962.** Studies on ferns (Filicineae). 2. The properties of a galactoglucomannan and a cellulose from cinnamon fern (*Osmunda cinnamomea*). *Svensk Papperstidning* 65: 173–177.
- Verhertbruggen Y, Marcus SE, Haeger A, Ordaz-Ortiz JJ, Knox JP. 2009.** An extended set of monoclonal antibodies to pectic homogalacturonan. *Carbohydrate Research* 344: 1858–1862.
- van Bergen PF, Hatcher PG, Boon JJ, Collinson ME, de Leeuw JW. 1997.** Macromolecular composition of the propagule wall of *Nelumbo nucifera*. *Phytochemistry* 45: 601–610.

Whistler RL, Chen CC. 1991. Hemicelluloses. *International Fiber Science Technology* **11**: 287–319.

Willats WGT, Marcus SE, Knox JP. 1998. Generation of a monoclonal antibody specific to (1→5)-β-L-arabinan. *Carbohydrate Research* **308**: 149–152.

Willats WGT, Steele-King CG, Marcus SE, Knox JP. 1999. Side chains of pectic polysaccharides are regulated in relation to cell proliferation and cell differentiation. *Plant Journal* **20**: 619–628.

Figure legends

Figure 1. Transverse vibratome sections through different regions of a large leaf of *A. rutifolium*. **A.** Overview of the leaf with indication of the positions of the sections (1–12; adaxial side of the leaf is facing upwards). All sections contain subepidermal collenchymatous tissue. Dark areas represent sclerified collenchymatous tissue, which is more abundant near the petiole base and absent in the upper part of the leaf. **B.** Detail of a section through the petiole base showing strands of sclerified collenchymatous tissues (s) surrounded by collenchymatous tissue (c). Scalebar B: 100 μm .

Figure 2. Transverse- (A, D, E) and longitudinal- (B, C) sections through the petiole of *A. rutifolium* stained with Delafield's heamatoxylin (A) and toluidine blue O (B–E).

A. The subepidermal collenchymatous tissue (c) is interrupted by parenchyma at the lateral respiration lines (arrows). The parenchyma tissue (p) consists of cortex parenchyma, enclosing two vascular bundles. **B.** The collenchymatous cells have tapering ends and are narrow and elongated; the cortical parenchyma tissue (p) is isodiametric to moderately elongated. **C.** a higher magnification showing collenchymatous cells divided by several thin-walled septae (arrowheads). **D.** Section through young petiole base showing undifferentiated (non-thickened) collenchymatous tissue (c) and parenchymatous tissue (p). **E.** Section through mature petiole base showing thickened collenchymatous (c) and parenchyma tissue (p). t: tracheids. Scale bars: A, 250 μm ; B, 100 μm ; C–E, 50 μm .

Figure 3. Indirect immunofluorescence detection of cell wall glycan epitopes in collenchymatous cell walls in transverse vibratome sections through petioles of *A. rutifolium*. **A.** Calcofluor White fluorescence showing full extent of cell walls. **B.** Binding of the cellulose-directed CBM3a probe to collenchymatous and parenchymatous cell walls. **C.** LM19, binding to pectic homogalacturonan with no or a low level of methylesterification shows similar binding patterns as CBM3a. **D.** LM20, directed against highly methyl-esterified pectic homogalacturonan, binds weakly to collenchymatous walls, but strongly to intercellular space linings of cortical parenchyma. **E, F.** Binding of LM19 and LM20 antibodies to collenchymatous cell walls in longitudinal sections. **G.** The LM5 galactan epitope was only detected in inner cell wall layers of collenchymatous tissue and in the septae (inset). **H.** LM6, recognizing arabinan, only weakly bound to epidermal cell walls. **I.** The anti-mixed-linkage glucan antibody BS-400-3 binds to the inner cell wall layers of the collenchymatous cells. **J.** Immunodetection of the xyloglucan LM25 epitope in collenchymatous walls. Note that antibody binding is stronger in the inner layer of the walls. **K.** Higher magnifications of the collenchymatous tissues show that Calcofluor White staining is brighter in the intercellular spaces. **L.** After pectate lyase treatment, LM15, recognizing the XXXG-motif of xyloglucan, binds to intercellular cell wall material. **M.** Combined image of Calcofluor White staining (blue) and LM15 binding (green). cp: cortical parenchyma. Scale bars: 50 μ m.

Figure 4. Indirect immunofluorescence detection of the LM21 heteromannan-epitope in Collenchymatous and sclerified Collenchymatous tissues. **A, B.** No binding of anti-mannan LM21 to collenchymatous (a) and cortical parenchyma- (b) cell walls. **C, D.** Pectate lyase pretreatment unmasked the LM21 epitope in primary cell

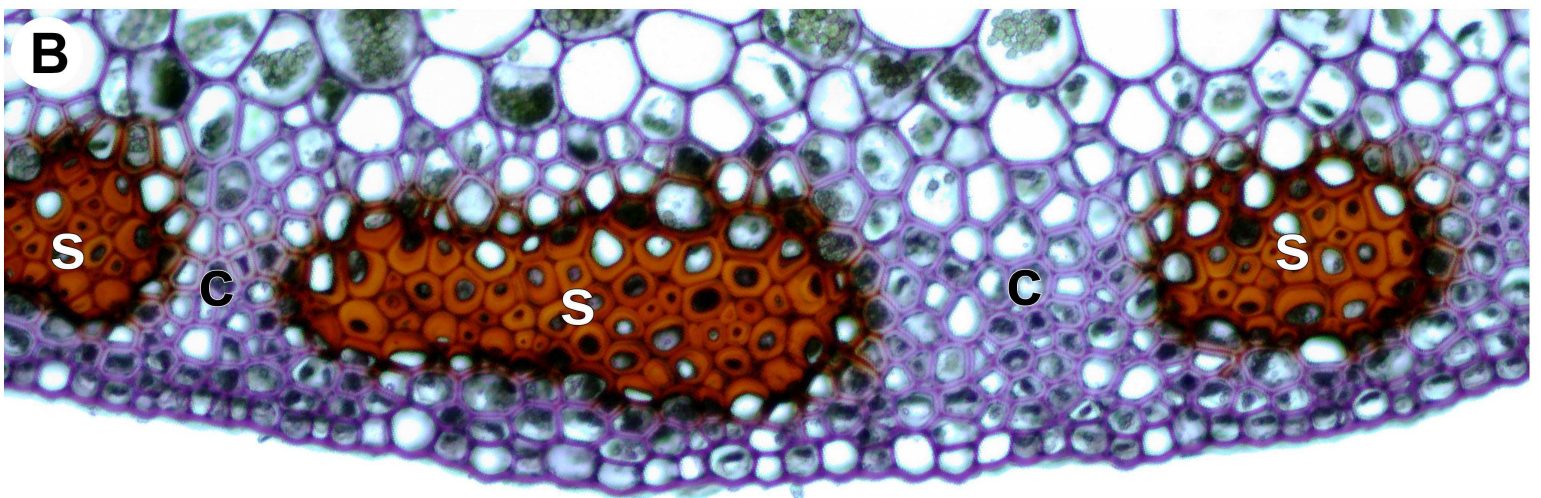
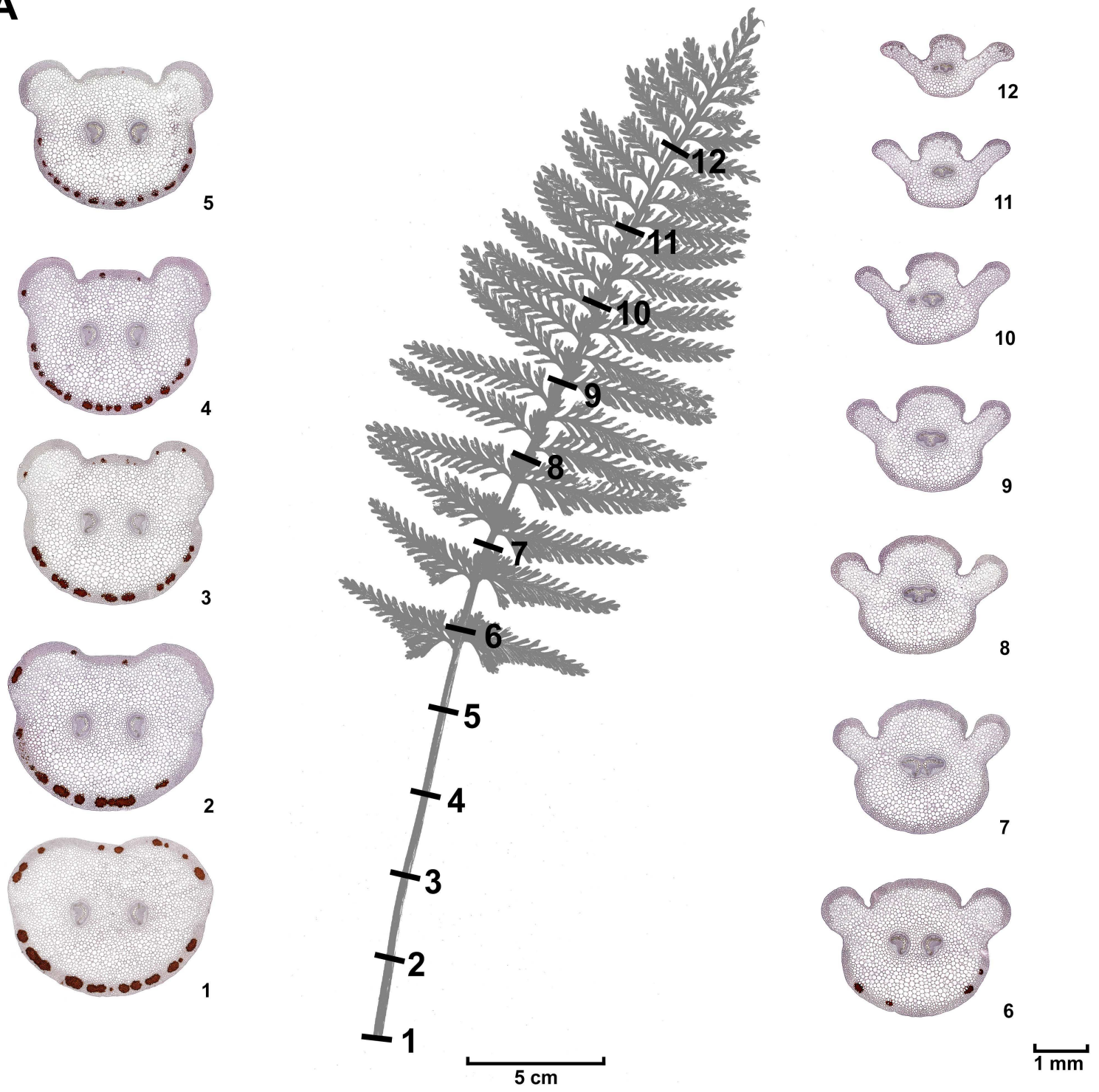
walls of collenchymatous (c) and parenchymatous (d) cell walls. A–D are combined images of antibody binding (green) and Calcofluor White staining (blue). **E, F.** The LM21 epitope is not detected in transverse cell walls of collenchymatous cell walls. **G–I.** Sclerified collenchymatous tissues do not stain with Calcofluor White (G), have a distinct inner wall layer labelled with LM21 (H) and have walls that exhibit red autofluorescence (I). **J–L.** Incorporation of mannan precedes impregnation of walls with dark-brown phenolic compounds, as LM21 labels sclerifying collenchymatous cells (J) while Calcofluor White staining (K) and absence of red autofluorescence (L) are observed in the same walls. Scale bars: 50 μm .

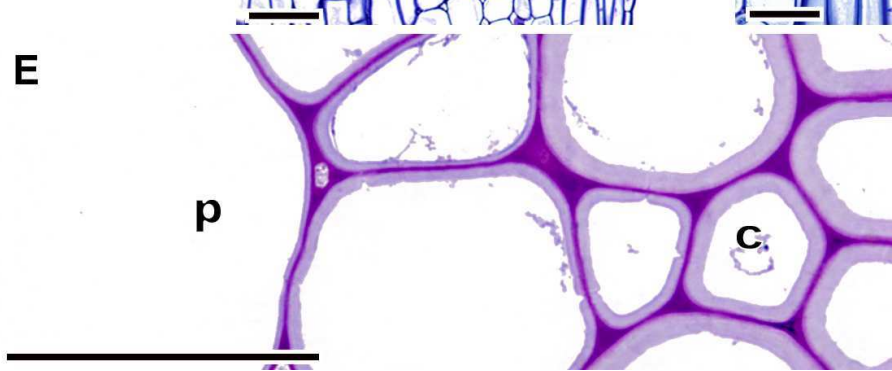
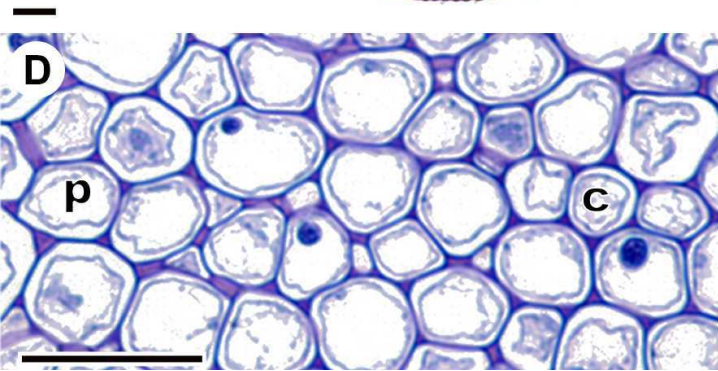
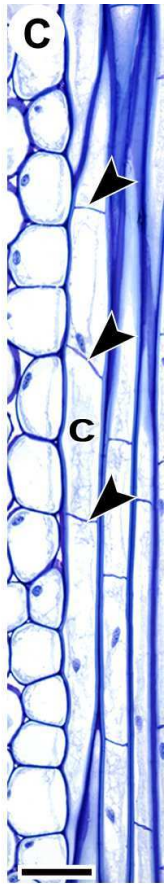
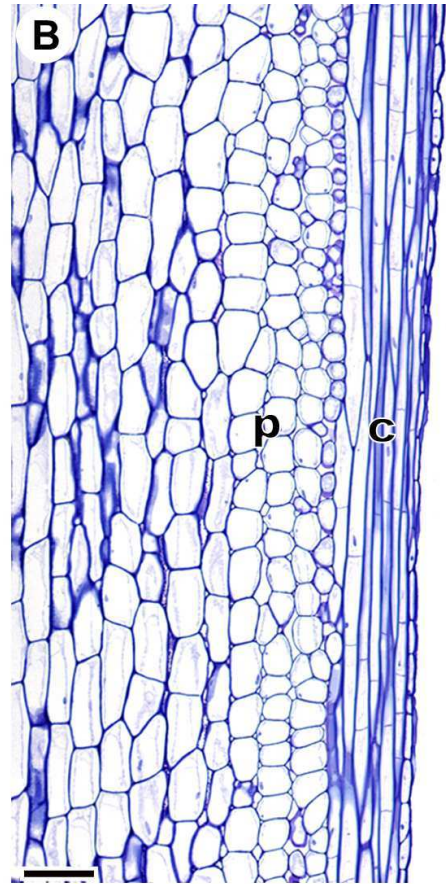
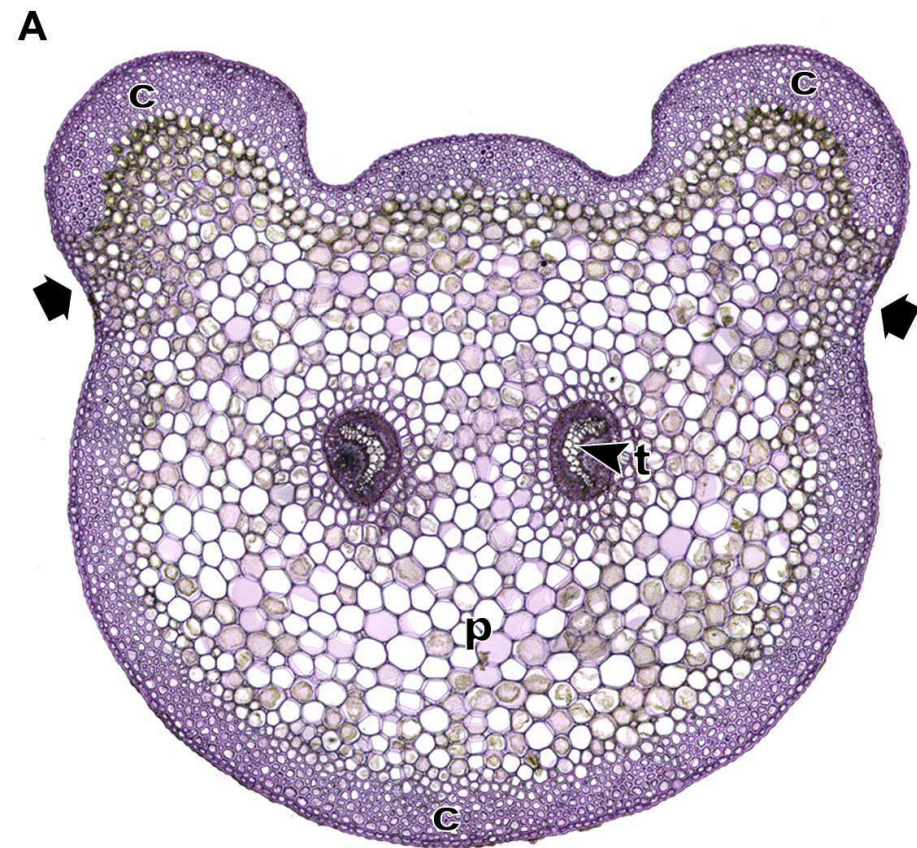
Figure 5. Ultrastructure and cellulose microfibril angle measurements of collenchymatous and sclerified collenchymatous tissue of *A. rutifolium*. **A.** Longitudinal section showing that collenchymatous walls are polylamellated with alternating electron-dense and electron-lucent lamellae. Middle lamellae and cell junctions are electron dense (asterisk). Septae remain thin-walled. **B.** A higher magnification shows that the middle lamella of the septa (arrowhead) does not fuse with that of the collenchymatous parent cell. The primary wall of the septa is continuous with the inner wall layer of the collenchymatous parent cell. **C.** Transverse section of sclerified collenchymatous tissue. Three zones can be distinguished in the secondary cell wall: the original collenchymatous wall impregnated with electron dense pigments ('1'), a thick electron dense layer deposited during sclerification ('2') and a thin electron lucent inner layer ('3'). **D.** scattering image of collenchyma. **E.** Scattering image of sclerified collenchymatous tissue. **F.** radial scattering profile of collenchyma (dark grey) and sclerified collenchymatous tissue (black). **G.** Azimuthal scattering profile of collenchyma (dark grey) and sclerified collenchymatous tissue (black). **H.**

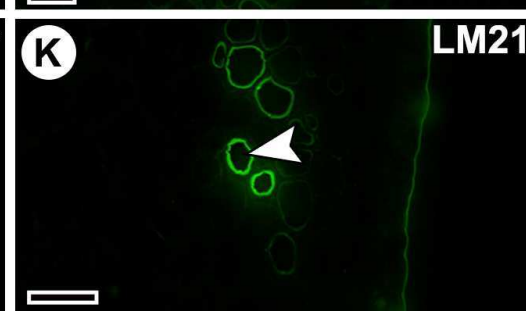
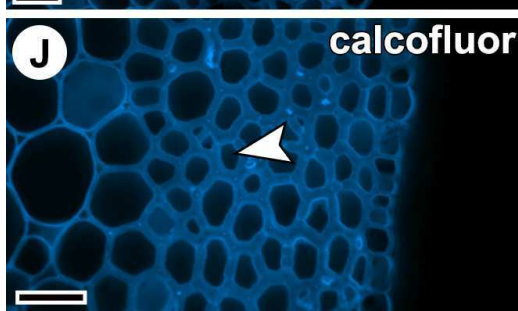
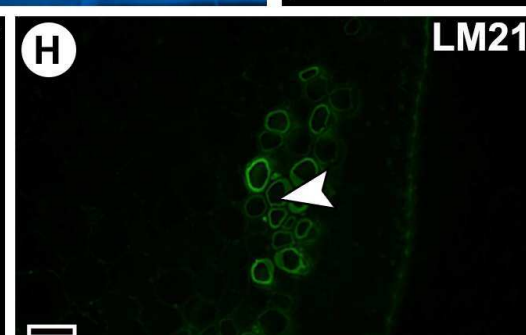
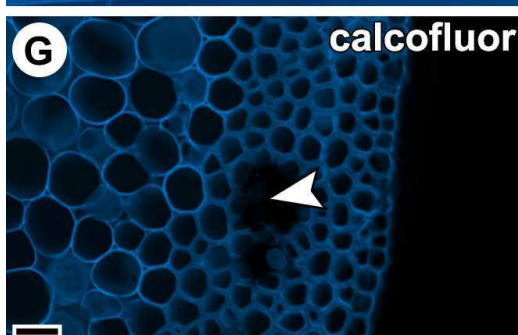
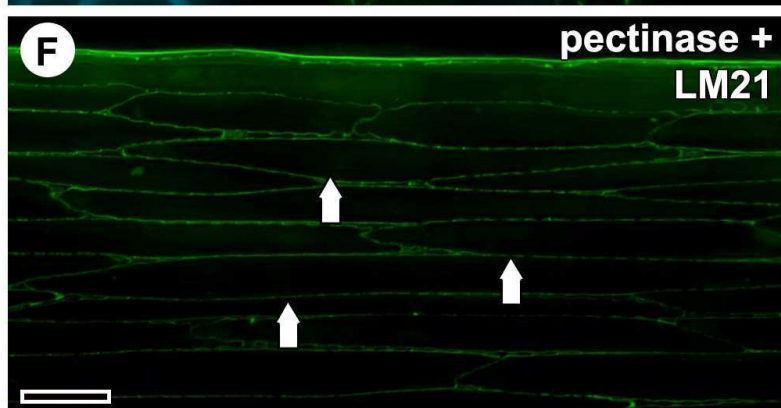
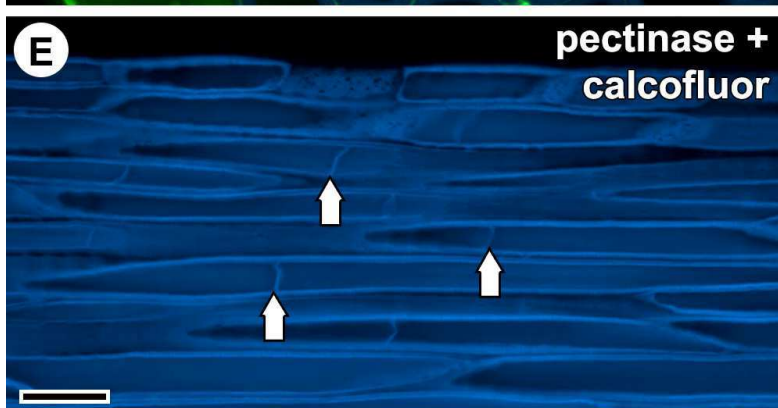
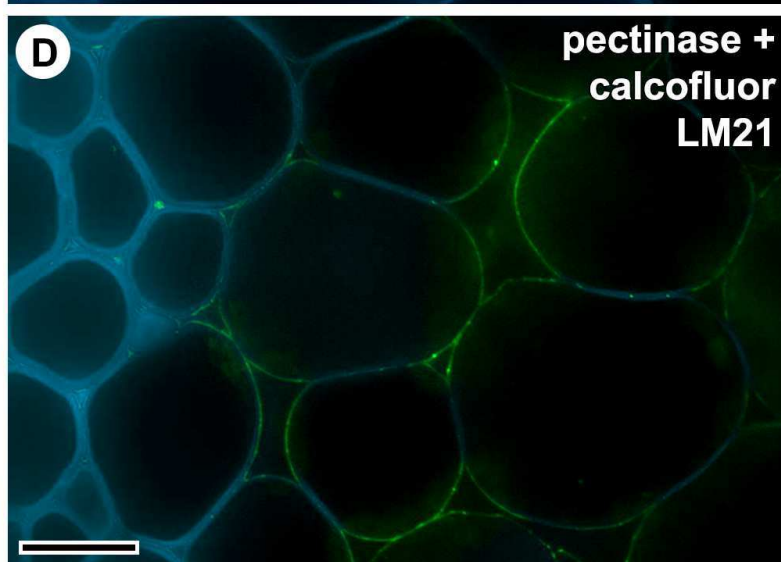
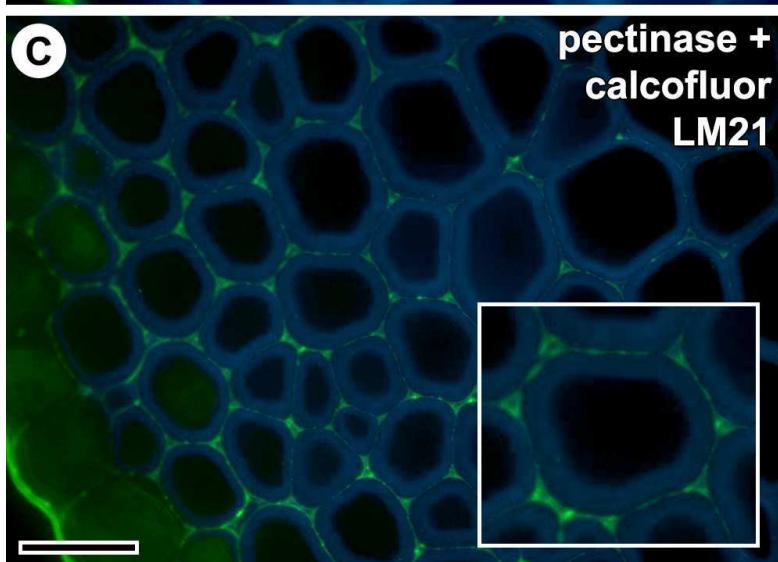
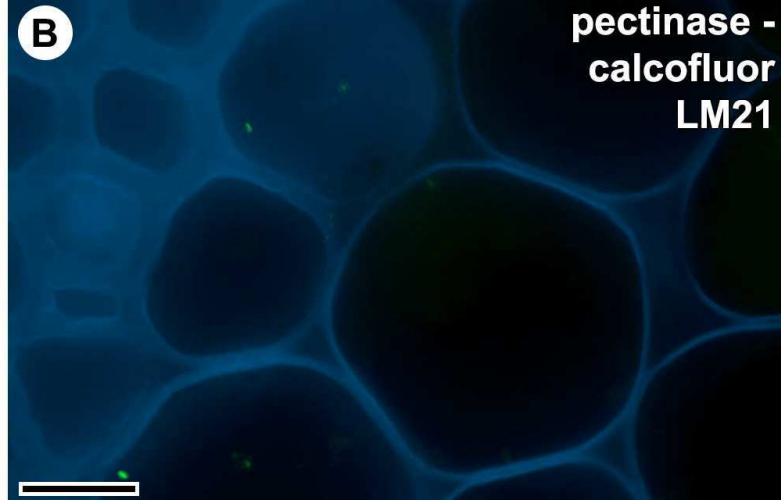
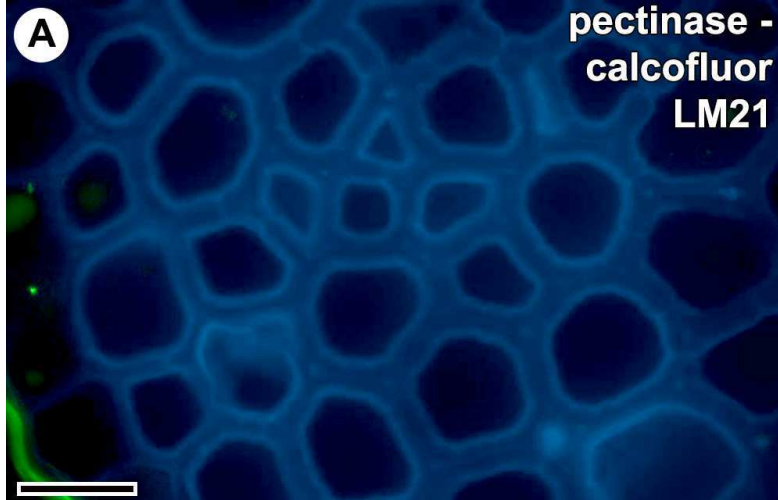
Simulated microfibril angle distribution of collenchyma (dark grey) and sclerified collenchymatous tissue (black). Scale bars: A, 2 μm ; B,C, 500 nm.

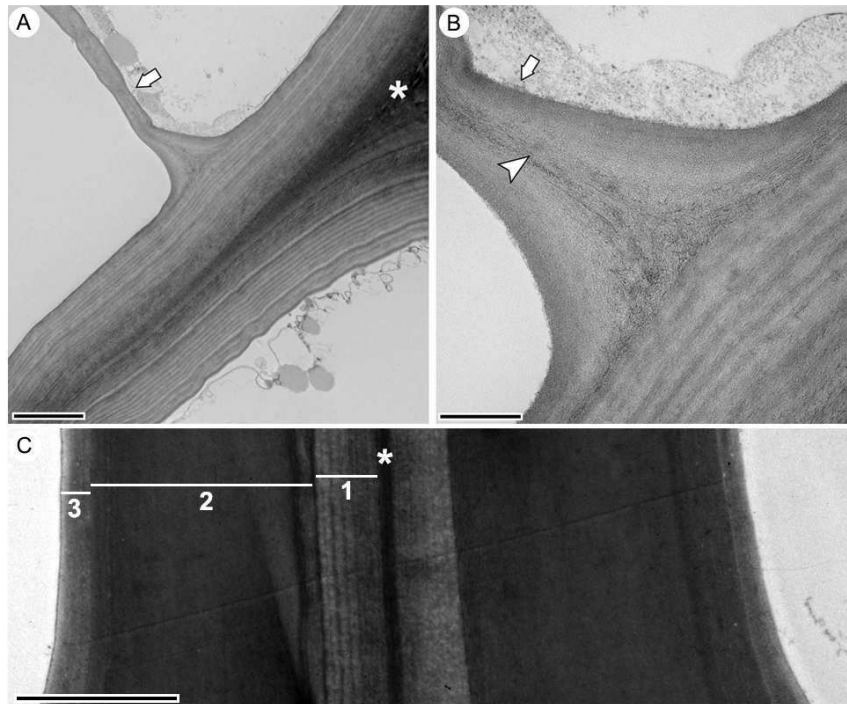
Figure 6. Nanoindentation experiments. The cartoon in the middle schematically shows a Berkovich indenter above a cell wall, indenting the cell wall and the final indent in the cell wall. **A.** Load function for sclerified collenchymatous cell walls. **B.** Load function for collenchymatous cells. **C.** Representative indentation curves with slope dP/dh for calculating E_r . **D.** E_r of sclerified collenchymatous cell walls (black) and collenchymatous cells walls (dark grey), **E.** Hardness of sclerified collenchymatous cell walls (black) and collenchymatous cells walls (dark grey).

Figure 7. Mechanical modeling. **A.** Segmented areas of petiole cross sections, light grey – parenchymatic tissue, dark grey – collenchyma and black – sclerified collenchymatous tissue. **B.** Plot of the calculated flexural stiffness of each section of the petiole versus position along the petiole, calculated both with and without the presence of sclerified collenchymatous tissue. Values of flexural stiffness are normalized by the Young's modulus of the collenchymatous tissue and are given in units of mm^{-1} .

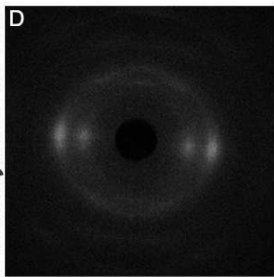
A



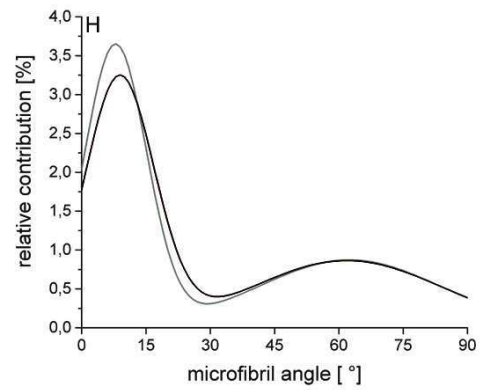
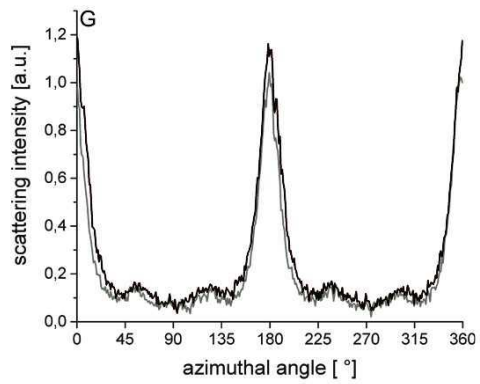
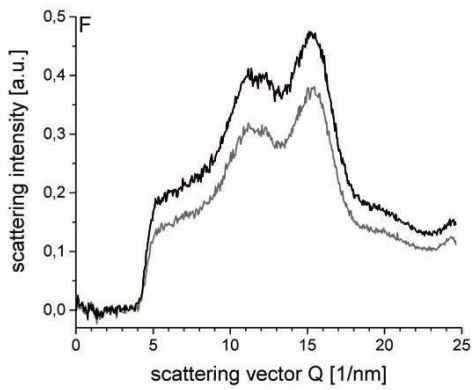
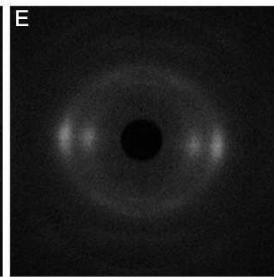




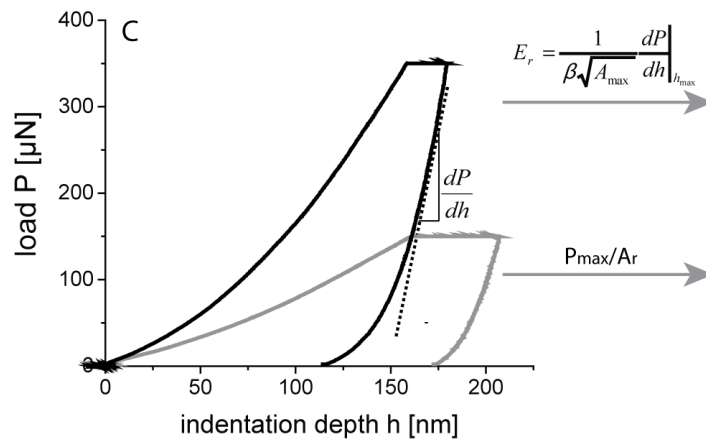
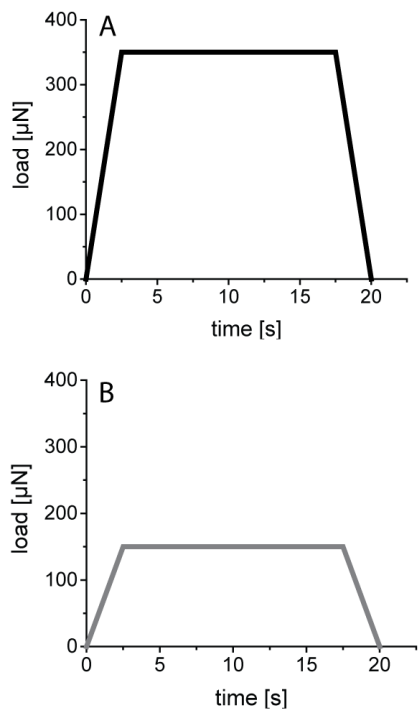
collenchymatous cells



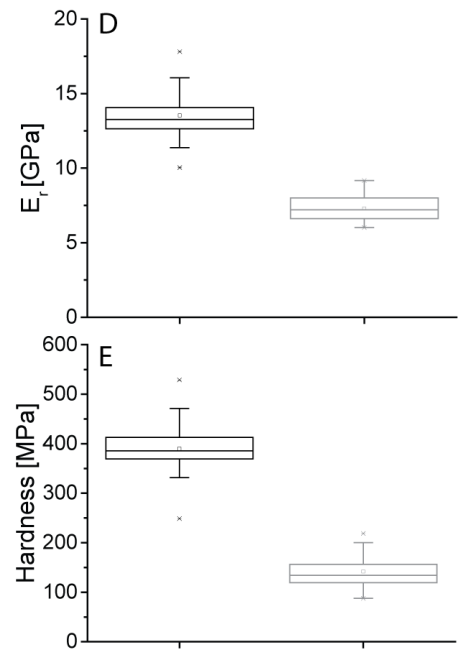
sclerified collenchymatous cells



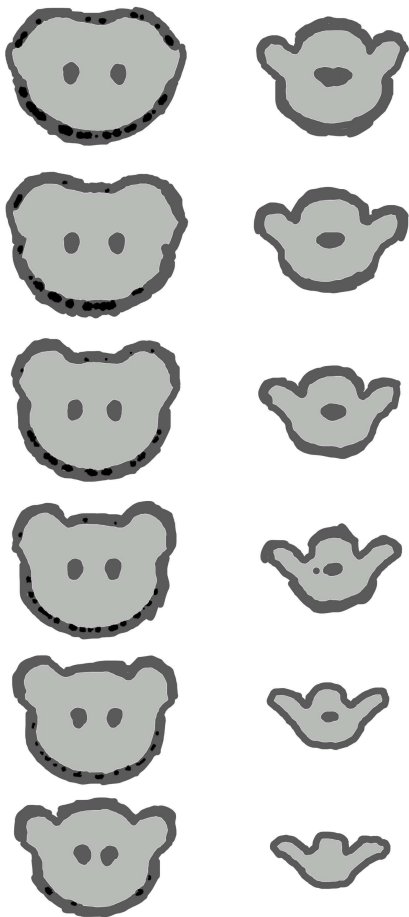
Load functions



Mechanical data



A Segmentation



B

